Dipole Response of Millennial Variability in Tropical South American Precipitation and $\delta^{18}O_p$ During the Last Deglaciation: Part II: $\delta^{18}O_p$ response

Yuntao Bao[1,2,*], Zhengyu Liu[1,*], Chengfei He[3]

1. *Department of Geography, The Ohio State University, Columbus, OH, USA*
2. *Laoshan Laboratory, Qingdao, China*
3. *Rosenstiel School of Marine, Atmospheric, and Earth Science, University of Miami, Miami, FL, USA*

*: *Corresponding authors: bao.291@osu.edu; liu.7022@osu.edu*

Journal of Climate

Resubmitted the revised manuscript (round 3)

Feb.19, 2023

Early Online Release: This preliminary version has been accepted for publication in *Journal of Climate*, may be fully cited, and has been assigned DOI 10.1175/JCLI-D-22-0289.1. The final typeset copyedited article will replace the EOR at the above DOI when it is published.

Abstract:

Understanding the hydroclimate representations of precipitation $\delta^{18}O$ ($\delta^{18}O_p$) in tropical South America (TSA) is crucial for climate reconstruction from available speleothem caves. Our preceding study (Part I) highlights a heterogeneous response in millennial hydroclimate over the TSA during the last deglaciation (20-11ka before the present), characterized by a northwest-southeast (NW-SE) dipole in both rainfall and $\delta^{18}O_p$, with opposite signs between central-western Amazon and eastern Brazil. Mechanisms of such $\delta^{18}O_p$ dipole response are further investigated in this study with the aid of moisture tagging simulations. In response to increased meltwater discharge, the Intertropical Convergence Zone (ITCZ) migrates southward, causing moisture source location shift and depleting the isotopic value of the vapor transported into eastern Brazil, which almost entirely contributes to the $\delta^{18}O_p$ depletion in eastern Brazil (SE pole). In contrast, moisture source location change and local condensation change (due to the lowering convergence level and increased rain reevaporation in unsaturated sub-cloud layers) contribute nearly equally to the $\delta^{18}O_p$ enrichment in the central-western Amazon (NW pole). Therefore, although a clear inverse relationship between $\delta^{18}O_p$ and rainfall in both dipole regions seems to support the "amount effect", we argue that the local rainfall amount only partially interprets the millennial $\delta^{18}O_p$ change in the central-western Amazon, while $\delta^{18}O_p$ does not document local rainfall change in eastern Brazil. Thus, the paleoclimate community should be cautious when using $\delta^{18}O_p$ as a proxy for past local precipitation in the TSA region. Finally, we discuss the discrepancy between the model and speleothem proxies on capturing the millennial $\delta^{18}O_p$ dipole response and pose a challenge in reconciling the discrepancy.

Significance statement

We want to comprehensively understand the hydroclimate footprints of $\delta^{18}O_p$ and the mechanisms of the millennial variability of $\delta^{18}O_p$ over tropical South America with the help of water tagging experiments performed by the isotope-enabled Community Earth System Model (iCESM). We argue that the millennial $\delta^{18}O_p$ change in eastern Brazil mainly documents the moisture source location change associated with ITCZ migration and the change of the isotopic value of the incoming water vapor, instead of the local rainfall amount. In contrast, the central-western Amazon partially documents the moisture source location shift and local precipitation change. Our study cautions that

Accepted for publication in *Journal of Climate*. DOI 10.1175/JCLI-D-22-0289.1.

one should not simply resort to the isotopic "amount effect" to reconstruct past precipitation in tropical regions without studying the mechanisms behind it.

1 Introduction

Stable water isotopologues are effective tracers of the hydrological cycle. Speleothems $\delta^{18}O$ ($\delta^{18}O_c$), as a powerful proxy, are widely used to reconstruct and trace past hydroclimate over tropical and subtropical regions due to their high temporal resolution and radiometric dating precision (Atsawawaranunt et al., 2018; Hu et al., 2019; He et al., 2021a). Most speleothem records that can be used to infer millennial variability in tropical South America (TSA) are located in the Andes and eastern Brazil regions, with few in the interior Amazon region. Thus, available speleothem $\delta^{18}O$ ($\delta^{18}O_c$) may not capture the complete picture of millennial hydroclimate change over the TSA. Our previous study (Part I) addressed this problem with a set of transient simulations during the last deglaciation performed on an isotope-enabled Earth system model. We highlight a heterogeneous response of a similar NW-SE dipole pattern, with opposite changes between central-western Amazon and eastern Brazil, in both millennial precipitation and $\delta^{18}O_p$, driven by meltwater forcing (Fig. 1). Our simulation is consistent with the results of multi-source paleoclimate proxy data, idealized snapshot, and idealized hosing experiments (Cruz et al., 2009; Cheng et al., 2013; Mohtadi et al., 2016; Campos et al., 2019). Possible mechanisms of the millennial dipole response in precipitation were also studied in Part I. The precipitation response is caused by a southward shift of ITCZ in response to increased meltwater forcing, with the ascending branch of the Hadley cell producing the low-level convergence and anomalous wet conditions in eastern Brazil (SE pole). In contrast, decreased easterly and anomalous subsidence is associated with a decreased Bolivia High, producing an abnormal dry condition in the central-western Amazon (NW pole), suggesting a decreased South American Summer Monsoon (SASM) intensity over the TSA. Here in Part II, we further study the mechanism of the dipole response of millennial $\delta^{18}O_p$ in detail.

Understanding the mechanisms of the $\delta^{18}O_p$ response requires the correct interpretation of the $\delta^{18}O_p$ representations of hydrological processes over the TSA. The isotopic "amount effect", i.e., increased local rainfall amount corresponds to much depleted $\delta^{18}O_p$, is widely believed to affect $\delta^{18}O_p$ values in tropical regions (Dansgaard, 1964) and is often used for rainfall reconstruction. Several studies have explained possible mechanisms (related to local vertical convective processes) for the

Accepted for publication in *Journal of Climate*. DOI 10.1175/JCLI-D-22-0289.1.

"amount effect", including the increased condensation and rainout with the increase of precipitation (Vuille et al., 2003), disequilibrium of raindrop with vapor based on relative humidity and raindrop size below the cloud base (Lee and Fung, 2007; Risi et al., 2008), raindrop reevaporatoin in an unsaturated downdraft (Worden et al., 2007; Risi et al., 2008), and the isotopic change of converged vapor associated with convective precipitation (Lee et al., 2007; Moore et al., 2014). The isotopic "amount effect" seems to exist in interannual (Vuille et al., 2003), millennial (Cruz et al., 2005; Cheng et al., 2013), and orbital precessional time scales (Cruz et al., 2009; Liu and Battisti, 2015) over the SASM region. However, the simple negative correlation between in situ $\delta^{18}O_p$ and rainfall amount may not be adequate to conclude the hydrologic representations of water isotopes, where the relationships with rainfall amount can be nonlocal and involve atmospheric processes that change the isotopic value of incoming water vapor (Lee et al., 2009; Samuels-Crow et al., 2014). The "amount effect" can be an interpretation of $\delta^{18}O_p$ change only if local convection processes dominate and the isotopic composition of incoming water vapor does not change too much. More and more isotope-enabled modeling studies show that precipitation isotopologues ($\delta^{18}O_p$ and δD_p) in the SASM region record large-scale atmospheric circulation processes, including the moisture source location change (Vuille et al., 2003) and upstream rainout (Lee et al., 2009; Samuels-Crow et al., 2014), as well as local evapotranspiration or continental recycling (Vuille et al., 2003; Wang et al., 2017). Nonetheless, none of these studies quantitatively disentangle different processes that may influence $\delta^{18}O_p$ value, such as local convective condensation, upstream effects, and moisture source location changes. Therefore, it is desirable to study the hydroclimate representation of $\delta^{18}O_p$ over the TSA (or the SASM region) comprehensively by tagging and tracking stable water isotopologues in our climate models. This will, in turn, help us clarify the mechanisms of the millennial dipole response of $\delta^{18}O_p$.

In this study, we aim to investigate the hydroclimate interpretations of $\delta^{18}O_p$ over the TSA by answering the main question: What is the mechanism of NW-SE dipole response of $\delta^{18}O_p$ to meltwater forcing during the last deglaciation? With the help of a state-of-art isotope-enabled Earth system model, we tag and track the movement and fractionation of $H_2{}^{18}O$ and $H_2{}^{16}O$ throughout the water lifecycle. This tagging technique helps us to identify what hydrological processes that $\delta^{18}O_p$ records and investigate the mechanisms responsible for the $\delta^{18}O_p$ dipole response in the TSA region (see Part I). Despite an inverse relationship between $\delta^{18}O_p$ and rainfall amount in both dipole regions, we argue that $\delta^{18}O_p$ only partially documents local rainfall change in the NW pole. On the other hand,

Accepted for publication in *Journal of Climate*. DOI 10.1175/JCLI-D-22-0289.1.

the SE pole $\delta^{18}O_p$ change mainly reflects the meridional migration of the ITCZ and the isotopic composition of the incoming water vapor, instead of local precipitation change. The changes in circulation associated with ITCZ migration lead to changes in relative moisture contribution from different source regions, which collectively cause the NW-SE dipole response pattern. Note that we will only focus on the austral summer of December-January-February (DJF), which dominates the annual $\delta^{18}O$ and precipitation changes over TSA (see Part I for detail). Similar to Part I, this study only focuses on the lowland TSA region, excluding the Andes that will be studied in the follow-up research.

2 Methods

2.1 The model

We use the state-of-the-art Community Atmosphere Model version 5.3 (Neale et al., 2010), which incorporates water isotopologues (iCAM5). iCAM5 is a component of the isotope-enabled version of the Community Earth System Model (iCESM) (Brady et al., 2019; Nusbaumer et al., 2017) and is on a 2.5° longitude and 1.9° latitude finite-volume grid with 30 hybrid vertical levels. The iCAM5 successfully captures the general features of precipitation isotope in observations in the present (Nusbaumer et al., 2017; Brady et al., 2019) and the past (He et al., 2021a, b) climate over the high latitude and Asian monsoon regions.

2.2 Water tagging simulations and analysis

To better understand moisture source and hydroclimate representation of $\delta^{18}O$ over the TSA region on the millennial time scale, we conducted two snapshot water tagging experiments at the Last Glacial Maximum (LGM; 20 ka) and Heinrich Stadial (HS1; 15.5 ka). The tagging experiments are carried out by the iCAM5 with the same settings as iTRACE simulations at LGM and HS1 (see methods in Part I). The atmospheric components are forced by the sea ice concentration, sea surface temperature, $\delta^{18}O$, and δD from the iTRACE simulations. Each tagging experiment is integrated for 40 years, with the last 20 years used for analysis. The tagging experiments reproduce the response to meltwater forcing (HS1 minus LGM) in the iTRACE simulation (He et al., 2021a, b). For the TSA region, the climatology and millennial hydroclimate response to meltwater forcing in the tagging experiments (Fig. 1) are very similar to that in iTRACE simulations (Fig1 and 4 in Part I).

Accepted for publication in *Journal of Climate*. DOI 10.1175/JCLI-D-22-0289.1.

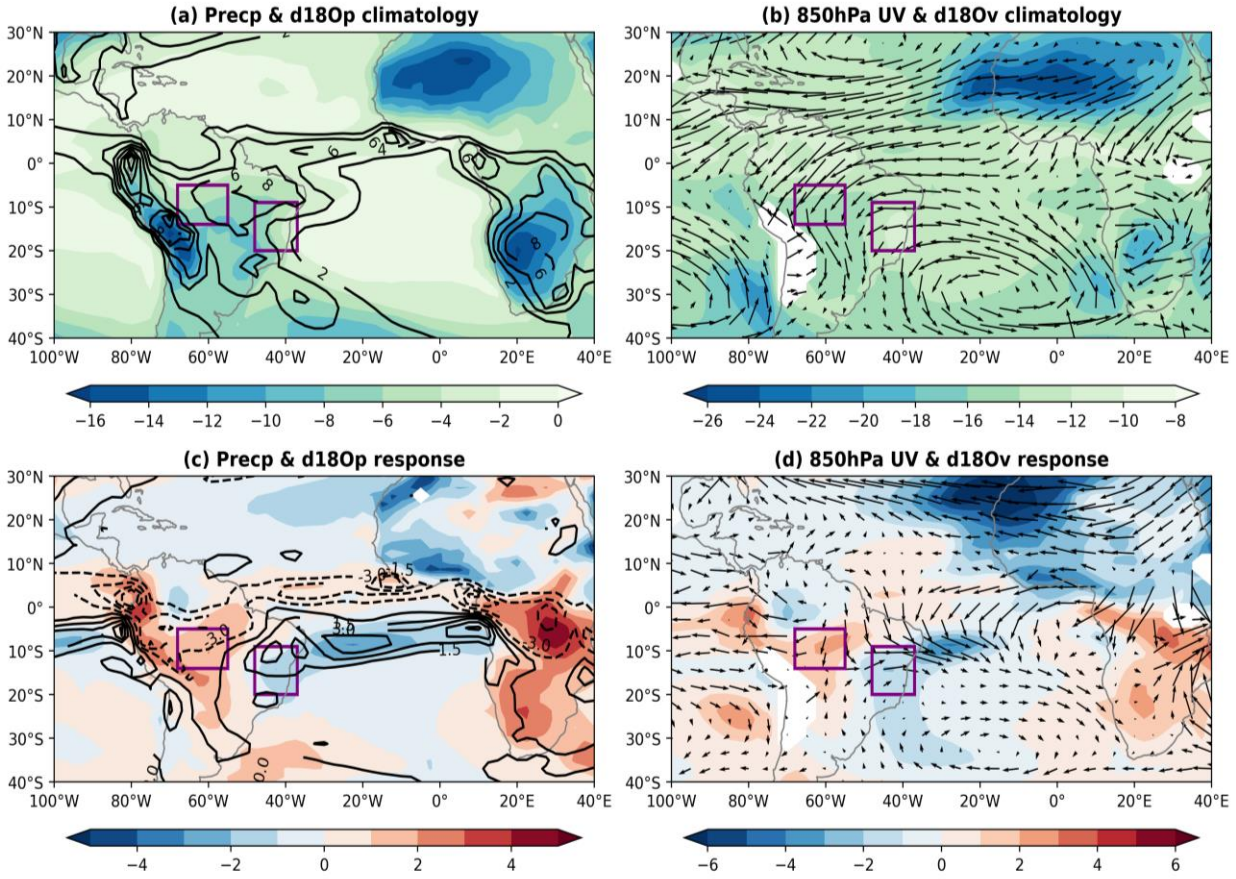

Fig. 1. Hydroclimate climatology at the LGM and hydroclimate response to meltwater forcing (HS1 minus LGM) in DJF for snapshot tagging simulation. (a) $\delta^{18}O_p$ (shading in *permil*) and precipitation (contours in *mm/day*); **(b)** $\delta^{18}O$ of vapor ($\delta^{18}O_v$) (shading in *permil*) and wind at 850hPa level (vectors in 3 *m/s*); **(c-d)** are similar to (a-b), but for the difference map between HS1 and LGM. The NW and SE $\delta^{18}O_p$ dipole regions are marked as purple polygons in a-d for reference.

For the purpose of this paper, the surface of the globe is divided into four moisture source regions (shown in Fig. 2a1-a3): 1. the subtropical northern and equatorial Atlantic Ocean (EQA); 2. the subtropical South Atlantic Ocean (SSA); 3. the continental South America (SAM); 4. the rest of the globe, denoted as "others." The total precipitation and $\delta^{18}O_p$ at a grid point are the sum of all four tagged source regions:

$$\delta^{18}O_p = \sum_{i=1}^{4} \delta^{18}O_{p,sink,i} \left(\frac{P_i}{P}\right) \text{ and } P = \sum_{i=1}^{4} P_i \quad (1)$$

where P_i and $\delta^{18}O_{p,sink,i}$ are precipitation and $\delta^{18}O_p$ at sink region originating from the tagged region *i*. The $\frac{P_i}{P}$ denotes the relative precipitation contribution from the tagged source region *i*.

Accepted for publication in *Journal of Climate*. DOI 10.1175/JCLI-D-22-0289.1.

We further decompose the life cycle of vapor ^{16}O and ^{18}O into different hydrological processes for each tagged source region. Following Tabor et al. (2018), the $\delta^{18}O_p$ from a tagged source region *i* can be decomposed approximately into three parts throughout its life cycle:

$$\delta^{18}O_{p,sink,i} = \delta^{18}O_{v,source,i} + \left(\delta^{18}O_{v,sink,i} - \delta^{18}O_{v,source,i}\right) + \left(\delta^{18}O_{p,sink,i} - \delta^{18}O_{v,sink,i}\right) \quad (2)$$

source composition *en route* *local condensation*

Here, $\delta^{18}O_{v,source,i}$ is the $\delta^{18}O$ of water vapor ($\delta^{18}O_v$) at the moisture source region *i* due to evaporation; $\delta^{18}O_{v,sink,i} - \delta^{18}O_{v,source,i}$ is the effect of en route depletion in $\delta^{18}O_v$ along the moisture trajectory from tagged source region *i* to the sink region; En route depletion is generally due to the upstream condensation and rainout depending on travel distance. The $\delta^{18}O_{p,sink,i} - \delta^{18}O_{v,sink,i}$ is the effect of local condensation change in $\delta^{18}O_p$ at the sink region, involving the physical processes of uplift condensation, rain re-evaporation within unsaturated downdraft, isotopic mixing and reequilibrium, and other microphysical processes.

Changes in sink region $\delta^{18}O_p$ that originates from a tagged source region *i*, or specifically, the millennial response of total $\delta^{18}O_p$ to meltwater flux (difference between HS1 and LGM), can be decomposed as follows:

$$\Delta\left(\delta^{18}O_{p,i}\right) = \Delta\left(\delta^{18}O_{p,sink,i} \times \frac{P_i}{P}\right) \approx \frac{P_i}{P} \times \Delta\delta^{18}O_{p,sink,i} + \delta^{18}O_{p,sink,i} \times \Delta\frac{P_i}{P} \quad (3a)$$

pure $\delta^{18}O_p$ composition change *moisture source location change*

where a relatively small second-order term is neglected, and the $\delta^{18}O_p$ response is assumed to be linear. Equation (3a) shows that the change of total $\delta^{18}O_p$ is contributed by the changes due to the pure $\delta^{18}O_p$ composition in the sink region ($\frac{P_i}{P} \times \Delta\delta^{18}O_{p,sink,i}$) and to the relative moisture contribution from each tagged region (in terms of relative contribution to the total rainfall) ($\delta^{18}O_{p,sink,i} \times \Delta\frac{P_i}{P}$). In general, the relative moisture contribution change indicates the moisture source location change. Note that the part of each term without changes (i.e., without the notation of Δ) represents the climatological mean state. Therefore, moisture source location changes also include the influence of the climate mean of $\delta^{18}O_{p,sink,i}$ in the sink region. The change of pure $\delta^{18}O_p$ composition in the sink region $\frac{P_i}{P} \times \Delta\delta^{18}O_{p,sink,i}$ can be further decomposed into the contributions from the change in $\delta^{18}O_v$ composition at the tagged source region (the first term in equation 3b), change in upstream rainout or en route depletion in $\delta^{18}O_v$ (the second term in equation 3b), and changes in the effect of local condensation enrichment in $\delta^{18}O_p$ at the sink region (the third term in equation 3b):

Accepted for publication in *Journal of Climate*. DOI 10.1175/JCLI-D-22-0289.1.

$$\frac{P_i}{P} \times \Delta\delta^{18}O_{p,sink,i} = \frac{P_i}{P} \times \Delta\delta^{18}O_{v,source,i} + \frac{P_i}{P} \times \Delta\left(\delta^{18}O_{v,sink,i} - \delta^{18}O_{v,source,i}\right) + \frac{P_i}{P} \times \Delta(\delta^{18}O_{p,sink,i} - \delta^{18}O_{v,sink,i}) \quad (3b)$$

source composition change *en route rainout change* *local condensation change*

Finally, local condensation change $\frac{P_i}{P} \times \Delta(\delta^{18}O_{p,sink,i} - \delta^{18}O_{v,sink,i})$ describes vertical conversion from water vapor to precipitation, involving several physical processes associated with the local "amount effect". This term can be further decomposed into two contributions:

$$\frac{P_i}{P} \times \Delta\left(\delta^{18}O_{p,sink,i} - \delta^{18}O_{v,sink,i}\right) = \frac{P_i}{P} \times \Delta\left(\delta^{18}O_{p,sink,i} - \delta^{18}O_{v,surf,i}\right) + \frac{P_i}{P} \times \Delta\left(\delta^{18}O_{v,surf,i} - \delta^{18}O_{v,sink,i}\right) \quad (3c)$$

The first term represents the effect of sub-cloud rain reevaporation. The second term represents the local water vapor convergence.

2.3 The Rayleigh distillation model

The Rayleigh distillation model assumes the condensate formed from saturated water vapor is immediately removed from an air parcel with a fractionation process removing the heavier ^{18}O preferentially, depleting the isotope ratios $R = {}^{18}O/{}^{16}O$ of the remaining vapor in an isotopic equilibrium process. This gives the equation of the Rayleigh fractionation model in equation 4 (Dansgaard, 1964; Noone, 2012):

$$dln(R) = (\alpha - 1)dlnq \quad (4)$$

where α is the temperature-dependent fractionation factor, and q is the saturated specific humidity. Physically, $\delta^{18}O_v$ is progressively depleted due to condensation and rainout with increased distance from the source region. It should be noted that a number of processes will deviate from the Rayleigh distillation behavior at low altitudes, notably the mixing between different originated air masses, remoistening processes due to land surface evapotranspiration and isotopic exchange in convective system (Worden et al., 2007; Lee et al., 2009; Risi et al., 2010; Samuels-Crow et al., 2014). These effects can be assessed from the discrepancy of the model $\delta^{18}O_v$ slope from the theoretical $\delta^{18}O_v$ slope predicted from the Rayleigh fractionation model.

3 Tagging Climatology and hydrological representations of $\delta^{18}O_p$

3.1 Moisture source

Accepted for publication in *Journal of Climate*. DOI 10.1175/JCLI-D-22-0289.1.

Water-tagging simulations track the exact moisture (^{16}O) sources of precipitation over the TSA region. Analysis of moisture sources for LGM climatology (Fig. 2a1-a4) indicates a primary moisture contribution from the subtropical South Atlantic Ocean (SSA) to precipitation in eastern Brazil (SE pole), while a primary moisture contribution from the subtropical North and equatorial Atlantic Ocean (EQA) to the central-western Amazon (NW pole) precipitation. Specifically, eastern Brazil receives monsoon precipitation ~55% from the SSA, ~24% from continental South America (SAM), and ~13% from the EQA, while the central-western Amazon receives precipitation ~54% from the EQA and ~30% from SAM. These moisture source contributions are consistent with the low-level wind and the associated moisture flux: one branch of easterly monsoon wind associated with the South Atlantic Subtropical High transports moisture from the South Atlantic towards eastern Brazil. The other branch of easterly transports moisture from the northern equatorial Atlantic into the central-western Amazon (Fig. 1b). A significant part of the moisture evaporating from continental South America returns to the land as precipitation, highlighting the role of continental convection and moisture recycling in the TSA, especially for the central-western Amazon.

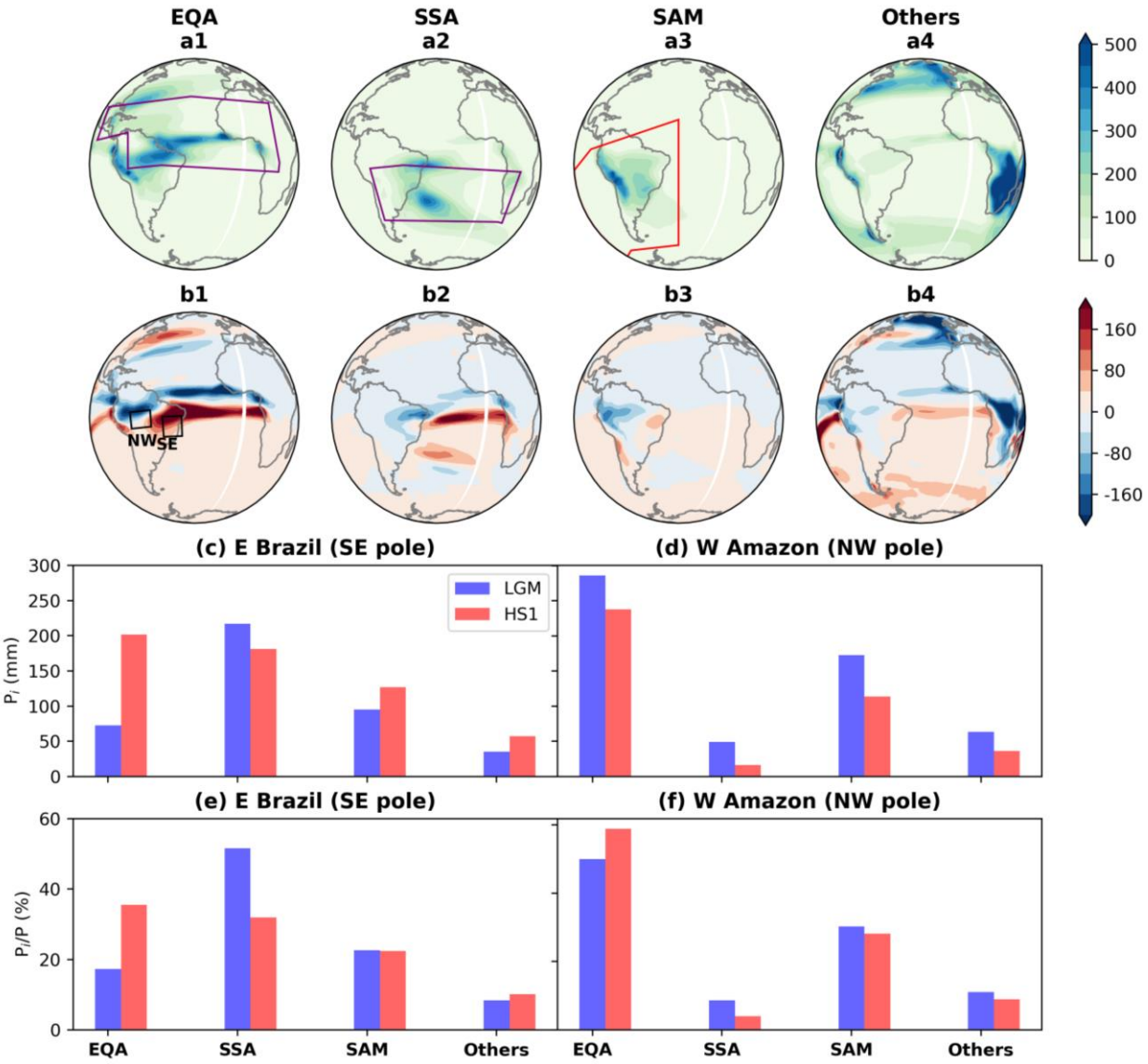

Fig. 2. Moisture (^{16}O) source tracking and its response to meltwater in DJF. **(a1-a4)** LGM climatological ^{16}O originating from moisture source region (a1) EQA, (a2) SSA, (a3) SAM, and (a4) other regions (units: *mm*). Polygons in a1-a3 mark the tagged source regions. **(b1-b4)** Same as (a1-a4) but for the difference between HS1 and LGM. **(c)** Eastern Brazil (48°W~37°W, 20°S~9°S) and **(d)** western Amazon (68°W~55°W, 14°S~5°S) precipitation originating from each moisture source (blue for LGM and red for HS1). Also shown are relative moisture contribution (%) from each source region to **(e)** eastern Brazil and **(f)** western Amazon. The NW and SE dipole regions of $\delta^{18}O_p$ are marked as black polygons in b1 for reference.

The origination of the $\delta^{18}O_p$ over the TSA (Fig. 3a1-5) is similar to the origination of moisture (^{16}O) at LGM (Fig. 2a1-4): SSA and EQA are the two major $\delta^{18}O_p$ source regions for eastern Brazil, while EQA provides the most portion of $\delta^{18}O_p$ for the central-western Amazon region. The $\delta^{18}O_p$ value is mostly negative if the precipitation moisture originates from a source with a long rainout

distance and heavy isotope depletion (Fig. 3a1-a2). In contrast, the SAM contributes a relative positive $\delta^{18}O_p$ value to the TSA, especially to the central-western Amazon region (Fig. 3a3), implying a large portion of convective rainfall (Worden et al., 2007; Aggarwal et al., 2016) and/or strong local evapotranspiration because the $\delta^{18}O_p$ signal is the most enriched if it precipitates over the local source (Vuille et al., 2003; Risi et al., 2010) where $\delta^{18}O_v$ comes from evapotranspiration without fractionation (Worden et al., 2007; Risi et al., 2010). It is also interesting to note that the eastern Pacific Ocean (included in "others" in Fig. 3) provides little $\delta^{18}O_p$ (< 2%) to the TSA region due to the terrain obstruction by the Andes Mountains despite a close geographical distance.

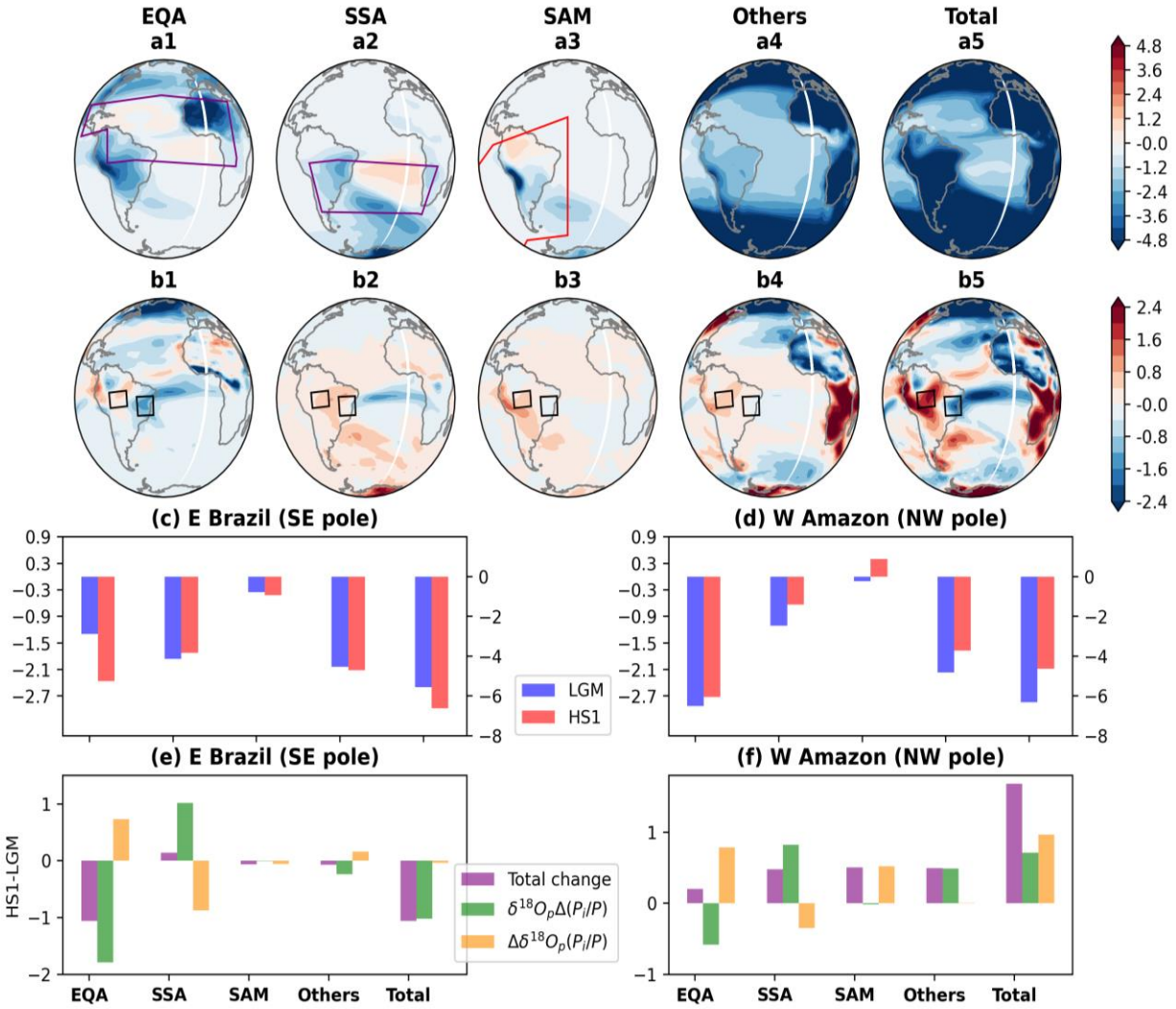

Fig. 3. Source tracking in $\delta^{18}O_p$ and its response to meltwater in DJF. (a1-a5) LGM climatological $\delta^{18}O_p$ originating from source region (a1) EQA, (a2) SSA, (a3) SAM, (a4) other regions, and (a5) global summation. Polygons in a1-a3 mark the tagging source regions. **(b1-b5)** Same as (a1-a5) but for the difference between HS1 and LGM. Climatological $\delta^{18}O_p$ of **(c)** eastern Brazil and the **(d)**

western Amazon that originate from different sources (blue for LGM and red for HS1). Also shown are the response of $\delta^{18}O_p$ to meltwater forcing (HS1 minus LGM) in **(e)** eastern Brazil and **(f)** western Amazon: total $\delta^{18}O_p$ change (purple) and $\delta^{18}O_p$ change due to relative moisture source location change ($\delta^{18}O_{p,sink,i}\Delta\frac{P_i}{P}$) (green) and pure $\delta^{18}O_p$ composition change ($\frac{P_i}{P}\Delta\delta^{18}O_{p,sink,i}$). The NW and SE dipole regions of $\delta^{18}O_p$ are marked as black polygons in b1-b5 for reference.

3.2 Hydrological representations of climatological $\delta^{18}O_p$

To understand the mechanisms of $\delta^{18}O_p$ dipole response over the TSA, we first examine hydrological representations of climatological $\delta^{18}O_p$ and clarify the effect of different water cycle components in determining the $\delta^{18}O$ composition.

We argue that climatological $\delta^{18}O_p$ evolution along the moisture trajectory does not represent the integral history of upstream condensation and rainout (en route depletion), as noted in equation 2. Instead, it represents the remoistening processes due to land evapotranspiration (continent moisture recycling) and vertical convection. We take the lower tropospheric moisture trajectory from EQA to the western Amazon (the NW pole trajectory) as an example. At LGM, the model climatological $\delta^{18}O_v$ deviates from the Rayleigh distillation theory significantly, with the model q-$\delta^{18}O_v$ in a semi-circle (Fig. 4a, c). This means that upstream rainout (or the so-called "continental effect") cannot interpret the spatial slope of $\delta^{18}O_v$, especially for the deep inland region. When moisture is transported from the coastal region inland to the western Amazon region, $\delta^{18}O_v$ (Fig. 4a) and $\delta^{18}O_p$ (Fig. 4e) remain little changed at first and then depleted, with the specific humidity first decreasing and then increasing (Fig. 4a). This implies that land evapotranspiration dominates the composition of $\delta^{18}O_v$ and $\delta^{18}O_p$ in coastal and eastern Amazon regions (east of 55°W), while remoistening from local convection probably dominates the $\delta^{18}O_v$ and $\delta^{18}O_p$ composition over the central-western Amazon region (west of 60°W). In contrast, at HS1, both $\delta^{18}O_v$ and $\delta^{18}O_p$ are more enriched in the mid-western Amazon and eastern flank of the Andes region (~65°W), and the associated mechanism will be discussed later. Our results are consistent with previous studies in that both continental evapotranspiration and local convection are important in the water cycle over the tropical continent (Worden et al., 2007; Risi et al., 2010).

Accepted for publication in *Journal of Climate*. DOI 10.1175/JCLI-D-22-0289.1.

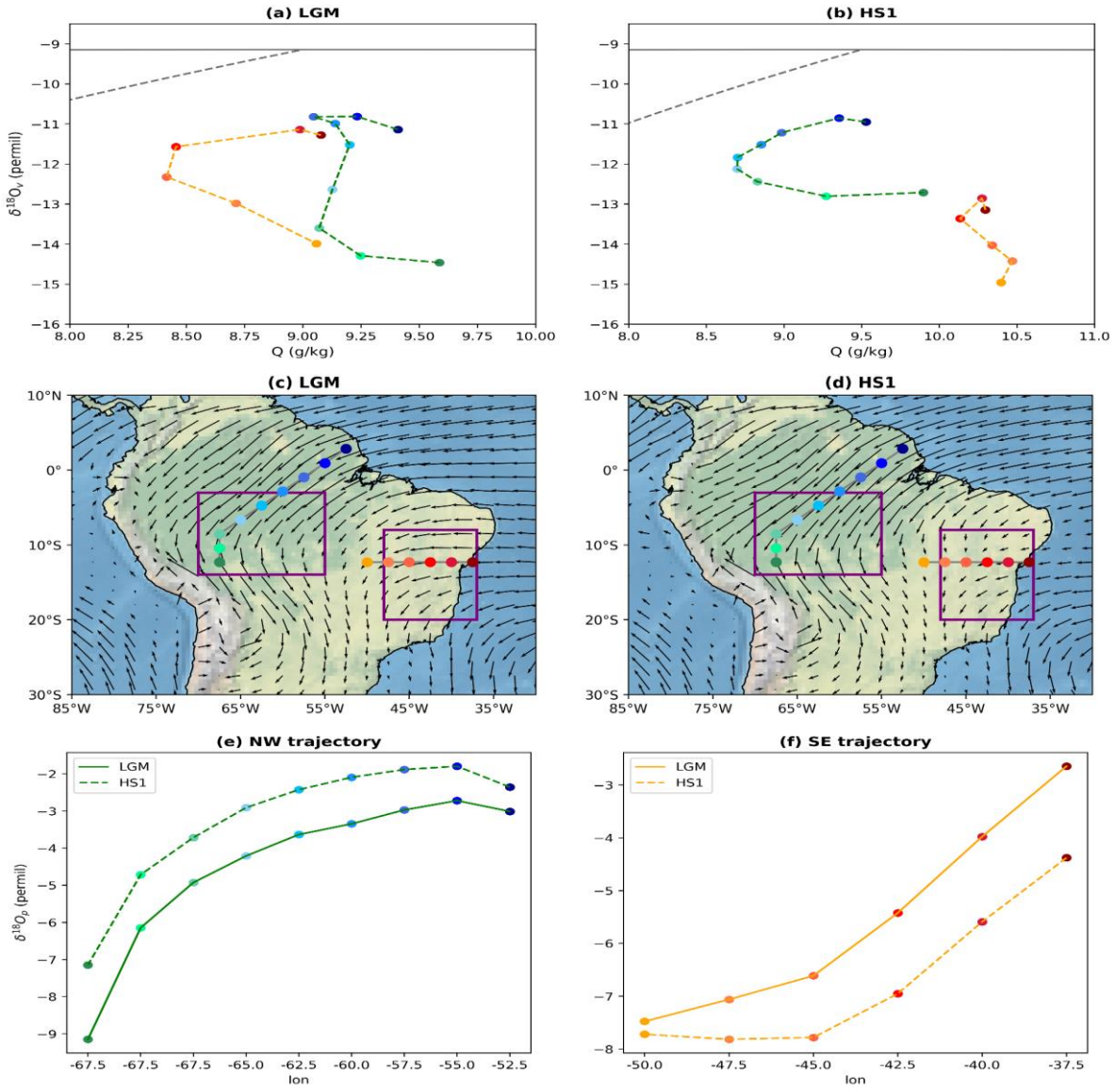

Fig. 4. Distribution diagram of DJF $\delta^{18}O_v$ and specific humidity along the moisture trajectory within the lower troposphere (950-850hPa) at (a) LGM and (b) HS1. Scatters with cool and warm colors are for climatology distribution along the NW pole and SE pole trajectories, respectively. Locations of each moisture trajectory are shown in **(c)** for LGM and **(d)** for HS1, overlayed with 850hPa wind. Also plotted are the theoretical Rayleigh fractionation curve (dashed grey line) and mixing curve (solid grey line) for reference. The theoretical air mixing line is calculated based on Noone (2012). **(e)** $\delta^{18}O_p$ along the NW pole moisture trajectory (solid and dashed lines are for LGM and HS1, respectively). **(f)** Similar to (e), but for SE pole moisture trajectory. The two $\delta^{18}O_p$ dipole regions are marked as purple polygons in c-d for reference.

4 Mechanism of $\delta^{18}O_p$ dipole response

Our simulations highlight a clear NW-SE dipole response (with opposite changes between central-western Amazon and eastern Brazil) in $\delta^{18}O_p$, with the millennial variation out of phase with rainfall in both poles (Fig. 1c). This inverse relationship between $\delta^{18}O_p$ and precipitation appears to

be consistent with isotopic "amount effect", as suggested previously (Dansgaard, 1964; Vuille et al., 2003; Cruz et al., 2005). However, our analysis of the TSA millennial $\delta^{18}O_p$ response reveals that this negative relationship can be nonlocal and involve atmospheric circulation processes that change the isotopic value of incoming water vapor and, therefore, no longer represent the local rainfall amount. For clarity, the local "amount effect" in this study refers to a negative relationship between $\delta^{18}O_p$ and rainfall amount at the same site caused by local vertical convection processes or excluding the remote effect of atmospheric circulation processes. To understand the mechanisms behind the millennial $\delta^{18}O_p$ dipole response, we separate the contributions of each hydrological process to sink region $\delta^{18}O_p$ change based on the water tagging decomposition method, which involves moisture source location change, moisture source composition change, en route rainout change, and condensation change, as shown in equation 3a and 3b. If the local rainfall amount is the main driver of millennial $\delta^{18}O_p$ change, we would expect a larger contribution of local condensation change to $\delta^{18}O_p$ change (Tabor et al., 2018). Here, we will show that the local condensation change partially contributes to the $\delta^{18}O_p$ change in the NW pole (or partially consistent with the local "amount effect"), while the moisture source location change (a remote effect instead of the local "amount effect") primarily contributes to $\delta^{18}O_p$ change in the SE pole, and thus produce the NW-SE dipole response in $\delta^{18}O_p$. Detailed analysis on $\delta^{18}O_p$ response to meltwater forcing (HS1 minus LGM) is as follows.

4.1 Factors controlling the millennial variability of $\delta^{18}O_p$

The change of moisture source location or relative precipitation contribution from different tagged regions, as represented by $\Delta\frac{P_i}{P}\delta^{18}O_{p,sink,i}$ in equation 3a, contributes to the NW-SE dipole of $\delta^{18}O_p$ (Fig. 5b5 versus a5), with a depleted $\delta^{18}O_p$ in eastern Brazil (SE pole) accompanying an enriched $\delta^{18}O_p$ in central-western Amazon (NW pole) (Fig. 5b5). With all source regions summed up, the moisture source location change ($\sum_{i=1}^{4}\Delta\frac{P_i}{P}\times\delta^{18}O_{p,sink,i}$) contributes almost the entire (~96%) to the $\delta^{18}O_p$ difference (-1.02‰ out of -1.06‰) in eastern Brazil (Fig. 3e), and contributes 44% to the total $\delta^{18}O_p$ difference (0.75‰ out of 1.72‰) in central-western Amazon (Fig. 3f). Therefore, millennial $\delta^{18}O_p$ change in eastern Brazil (SE pole) documents exclusively the change of moisture source location associated with atmospheric circulation processes. As a response to increased

Accepted for publication in *Journal of Climate*. DOI 10.1175/JCLI-D-22-0289.1.

meltwater forcing, the ITCZ migrates southward and significantly increases the moisture originating from EQA, such that the moisture contribution from EQA overwhelms that from SSA and becomes the primary moisture source (Fig. 2c, e; Fig. 3c, e). The EQA contributes more depleted $\delta^{18}O_p$ to eastern Brazil for two reasons: First, the evaporated $\delta^{18}O_v$ is more depleted over EQA than over SSA (Fig. 1b). Second, the moisture originating from the EQA travels a longer distance than from the SSA, further enhancing the upstream rainout depletion before reaching eastern Brazil (Fig. 3b1). As the dominant moisture source changes from SSA (for LGM) to EQA (for HS1) (Fig.5b1 vs. b2; Fig. 3e), the more depleted incoming $\delta^{18}O_v$ converges in the eastern Brazil region (Table 1), resulting in a net depletion in the total $\delta^{18}O_p$ over eastern Brazil sink region (Fig. 5b5).

Unlike eastern Brazil, where $\delta^{18}O_p$ documents exclusively the moisture source location change, the central-western Amazon (NW pole) documents less signal from moisture source location change (44% to the total change). Reduced moisture contribution from SSA and other sources (comparing HS1 with LGM: Fig. 2f; Fig. 3d, f) only partially contributes to the enriched $\delta^{18}O_p$ in the central-western Amazon (Fig. 5b5 versus a5) due to decreased low-level easterly wind. Additionally, pure $\delta^{18}O_p$ composition enrichment in the sink region, as represented by $\frac{P_i}{P} \times \Delta\delta^{18}O_{p,sink,i}$ in equation 3a, also contributes to the total $\delta^{18}O_p$ enrichment in the central-western Amazon (Fig. 5a5 versus c5). Quantitatively, with all the contributions from all sources summed up, the change of pure $\delta^{18}O_p$ composition ($\sum_{i=1}^{4} \frac{P_i}{P} \times \Delta\delta^{18}O_{p,sink,i}$) in the sink region contributes 56% to the total millennial $\delta^{18}O_p$ response in the central-western Amazon (0.96‰ out of 1.72‰). Further decomposition of pure $\delta^{18}O_p$ composition change in the sink region (based on equation 3b) indicates that local condensation $\frac{P_i}{P}\Delta(\delta^{18}O_{p,sink,i} - \delta^{18}O_{v,sink,i})$ and enroute/upstream rainout change $\frac{P_i}{P}\Delta\left(\delta^{18}O_{v,sink,i} - \delta^{18}O_{v,source,i}\right)$ determine the $\delta^{18}O_p$ values in the central-western Amazon region. Local condensation change enriches $\delta^{18}O_p$ by 0.84‰ out of 1.72‰, indicating that the local "amount effect" interprets about half of the total $\delta^{18}O_p$ change. The decreased upstream rainout enriches $\delta^{18}O_p$ by 0.56‰ out of 1.72‰, as the weakened low-level easterly (Fig. 1d) transports less moisture and suppresses condensation and rainout from the upstream regions towards the central-western Amazon.

To summarize, in response to meltwater forcing, the change of moisture source location due to the ITCZ migration almost entirely contributes to the millennial $\delta^{18}O_p$ response in eastern Brazil (SE pole), which is close to the Atlantic Ocean moisture source. In contrast, the contribution of the change

Accepted for publication in *Journal of Climate*. DOI 10.1175/JCLI-D-22-0289.1.

in moisture source location and local condensation to the millennial $\delta^{18}O_p$ response is almost equal in the inland central-western Amazon region (NW pole).

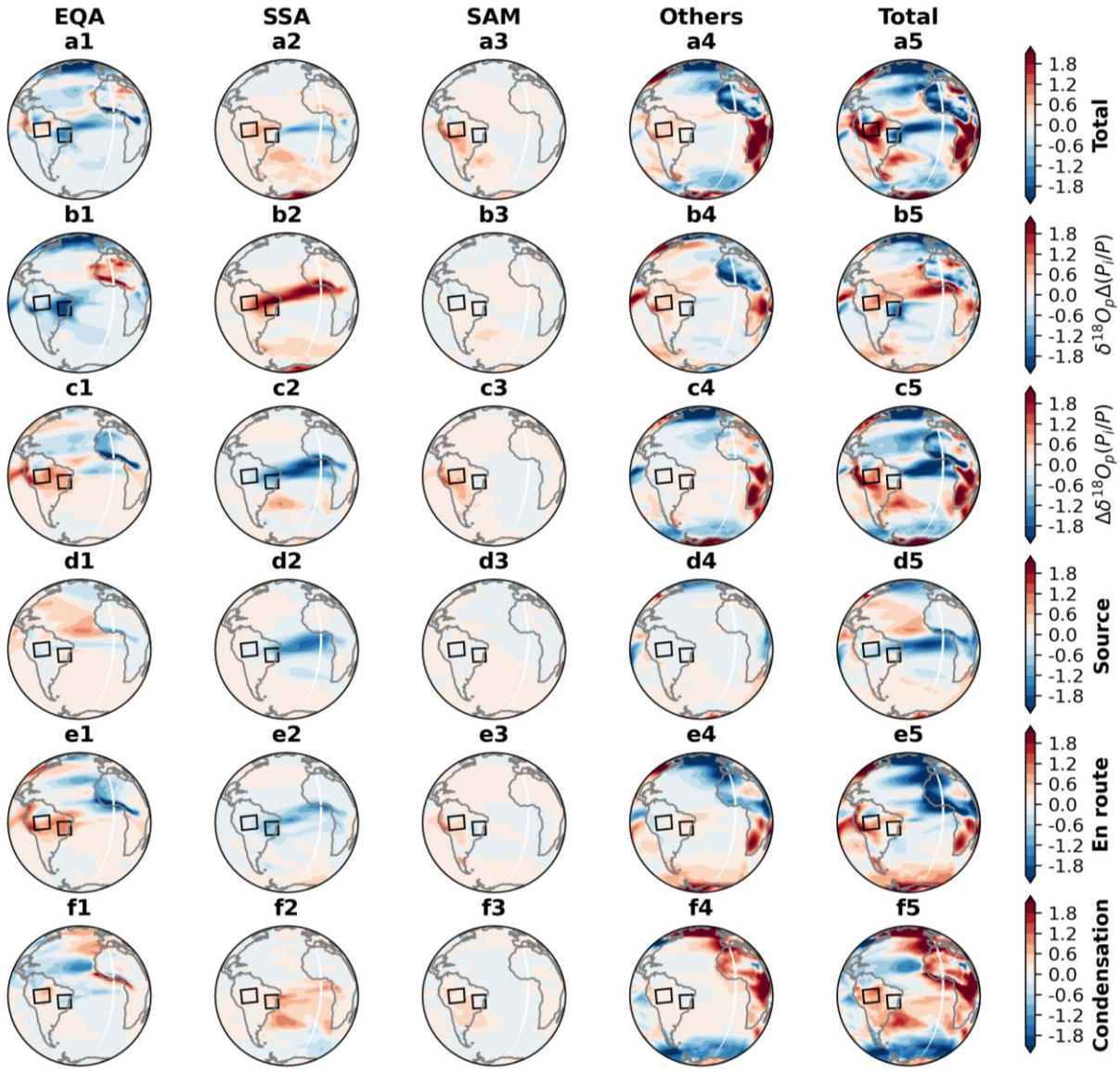

Fig. 5. Decomposition of $\delta^{18}O_p$ response from source regions (HS1-LGM) in DJF. Total $\delta^{18}O_p$ response originating from source region **(a1)** North and the equatorial Atlantic Ocean, **(a2)** South Atlantic Ocean, **(a3)** South America, **(a4)** other regions, and **(a5)** global summation. **(b1-b5)** Same as (a1-a7), but for response due to the change of moisture source location; **(c1-c5)** response due to pure $\delta^{18}O_p$ composition change, which is further decomposed to response due to the change of **(d1-d5)** $\delta^{18}O_v$ in the source region; **(e1-e5)** the en route depletion of $\delta^{18}O_v$; **(f1-f5)** condensation enrichment. The two $\delta^{18}O_p$ dipole regions are marked as black polygons for reference.

4.2 Moisture budget perspective of $\delta^{18}O_p$ interpretation on the "amount effect"

Although the clear inverse relationship between $\delta^{18}O_p$ and rainfall amount in both SE and NW poles seems to support the "amount effect", our analysis of water tagging decomposition indicated that the "amount effect" only partially interprets the millennial $\delta^{18}O_p$ change in the NW pole (~48% to the total change), while it does not interpret $\delta^{18}O_p$ change in the SE pole. This argument contradicts the widely accepted view that $\delta^{18}O_p$ largely represents local rainfall amounts in tropical regions and is commonly used to infer the past precipitation by paleoclimate communities. The moisture budget perspective (Table 1) further shows that the incoming vapor has a different isotopic value between LGM and HS1 in both poles due to the change of moisture source location. Therefore, $\delta^{18}O_p$ cannot be used to directly estimate local precipitation amount as it also documents the incoming water vapor isotopic composition associated with large-scale atmospheric circulation. Specifically, depletion of incoming $\delta^{18}O_v$ in the SE pole (geographically close to moisture source region), due to relative moisture source location change from SSA to EQA, largely accounts for the depletion of $\delta^{18}O_p$ (relative change of $\delta^{18}O_v$ and $\delta^{18}O_p$ are equivalent as is shown in Table 1) as the incoming $\delta^{18}O_v$ does not deplete too much during the local convergence. For the NW pole, enrichment of incoming $\delta^{18}O_v$, due to moisture source location change and decreased upstream rainout, partially explains the enrichment of $\delta^{18}O_p$. However, a larger contribution comes from anomalous local moisture convergence (Table 1 and Fig. 6) associated with the "amount effect", to be discussed later. It is worth noting that although evapotranspiration is important in determining the climatological spatial distribution of the $\delta^{18}O_p$ (discussed in section 3.2), it is not important to the local $\delta^{18}O_p$ change, especially for the NW pole (Table 1).

Here, we find two possible mechanisms behind the partial "amount effect" in the NW pole by further decomposing the local condensation change. Figure 6b gives the decomposed response (HS1 minus LGM) of local condensation change $\frac{P_i}{P}\Delta(\delta^{18}O_{p,sink,i} - \delta^{18}O_{v,sink,i})$ (equation 3c). It turns out that the increase of $\frac{P_i}{P}\Delta(\delta^{18}O_{v,surf,i} - \delta^{18}O_{v,sink,i})$ due to lowering convergence level and/or decreased local moisture convergence, and increase of $\frac{P_i}{P}\Delta(\delta^{18}O_{p,sink,i} - \delta^{18}O_{v,surf,i})$ due to increased sub-cloud rain reevaporation are two possible mechanisms that account for the positive local condensation change and thus the enrichment of $\delta^{18}O_p$. Physically, decreased convection corresponds to a lowering height of the maximum vertical velocity (or convergence) from 500hPa to 600hPa (Fig. 6c). Since the profile of $\delta^{18}O_v$ becomes more depleted with height, the decrease of maximum convergence height produces

Accepted for publication in *Journal of Climate*. DOI 10.1175/JCLI-D-22-0289.1.

enriched $\delta^{18}O_v$ in the mid and lower troposphere (Moore et al., 2014), and thus a larger departure of near-surface $\delta^{18}O_v$ from column $\delta^{18}O_v$, or, a positive $\frac{P_i}{P}\Delta(\delta^{18}O_{v,surf,i} - \delta^{18}O_{v,sink,i})$. Moreover, rain reevaporation and isotopic exchanges may lead to a local departure of $\delta^{18}O_p$ compared to near-surface $\delta^{18}O_v$. Thus, a larger $\frac{P_i}{P}\Delta(\delta^{18}O_{p,sink,i} - \delta^{18}O_{v,surf,i})$ indicates an increased rain reevaporation within a drier (decreased relative humidity shown in Fig. 6a) boundary layer.

Although possible mechanisms are given for partial "amount effect" in the NW pole region based on existing model output, we should note that the isotopic fractionation during condensation, deposition, re-evaporation, entrainment, and detrainment processes are described in the iCAM5 convection and cloud microphysics schemes (Nusbaumer et al., 2017). Thus, it is possible to directly investigate the mechanisms of the local "amount effect" by conducting sensitivity experiments for each process of fractionation in further study.

Table 1. Moisture budgets diagnose on water vapor flux, precipitation, and evaporation in eastern Brazil (SE pole) and central-western Amazon (NW pole), together with the isotopic composition of precipitation, evaporation, and vapor fluxes.

	SE pole			**NW pole**		
	LGM	**HS1**	**HS1-LGM**	**LGM**	**HS1**	**HS1-LGM**
P (mm/day)	4.6	6.3	1.7 (35%)	6.4	4.5	-1.9 (30%)
$\boldsymbol{q_{Fi}}$ (kg/m/s)	122.6	124.8	2.2 (2%)	154.0	187.5	33.5 (22%)
$\boldsymbol{q_{Fnet}}$ (kg/m/s)	13.6	1.7	-11.9 (87%)	-19.7	-16.1	3.6 (18%)
$\boldsymbol{\delta^{18}O_p}$ (‰)	-5.4	-6.4	-1.0 (18%)	-6.2	-4.6	1.6 (26%)
$\boldsymbol{\delta^{18}O_{Fi}}$ (‰)	-11.7	-13.4	-1.7 (14%)	-27.6	-26.4	1.2 (5%)
$\boldsymbol{\delta^{18}O_{Fet}}$ (‰)	-32.8	-30.1	2.7 (8%)	1.1	-0.3	-1.4 (127%)
E (mm/day)	2.4	2.3	-0.1 (4%)	2.5	2.4	-0.1 (4%)
$\boldsymbol{\delta^{18}O_{evap}}$ (‰)	-6.3	-6.8	-0.5 (8%)	-4.9	-4.8	0.1 (2%)

P is precipitation; q_{Fi} is moisture flux into the SE and NW pole regions; q_{Fnet} is net moisture flux within the SE and NW pole regions (calculated by the difference between outgoing and incoming moisture flux); $\delta^{18}O_p$ is $\delta^{18}O$ in precipitation; $\delta^{18}O_{Fi}$ is $\delta^{18}O$ of incoming vapor flux; $\delta^{18}O_{Fet}$ is $\delta^{18}O$ of net vapor flux; E is evapotranspiration; $\delta^{18}O_{evap}$ is $\delta^{18}O$ in evapotranspiration. The box regions of the SE and NW poles are shown as purple polygons in Fig. 1.

Accepted for publication in *Journal of Climate*. DOI 10.1175/JCLI-D-22-0289.1.

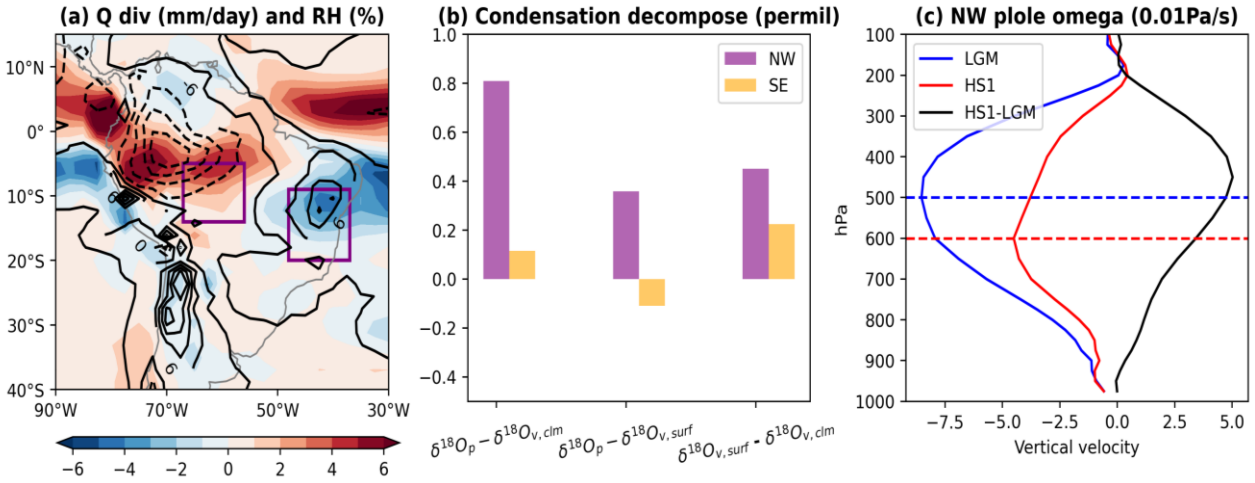

Fig. 6 (a) Difference map of precipitable water (shading: mm/day) and near-surface relative humidity (contours: %) between HS1 and LGM; **(b)** decomposition of local condensation change $\frac{P_i}{P}\Delta(\delta^{18}O_{p,sink,i} - \delta^{18}O_{v,sink,i})$ in the NW pole (purple) and SE pole (orange); **(c)** profiles of vertical velocity in the NW pole at LGM (solid blue line), HS1 (solid red line), and their difference (HS1-LGM: solid black line). Dashed blue and red lines are for levels of maximum vertical velocity, respectively.

5 Conclusion and Discussion

In this study, we investigated the hydroclimate footprint and the mechanism for the millennial dipole response of $\delta^{18}O_p$ over the TSA in the iCAM5 model implemented with a water-tagging technique. The mechanism of millennial $\delta^{18}O_p$ dipole response to increased meltwater forcing (HS1 minus LGM) is summarized schematically in Fig.7. Increased meltwater discharge produces southward migration of the ITCZ and reduction of the SASM circulation, causing the switch of moisture source location from SSA to EQA, and the depletion of isotopic value of the incoming water vapor (due to the import of more depleted $\delta^{18}O_v$ originating from the EQA and the increased distance of upstream rainout) to eastern Brazil region. The moisture source location change almost entirely contributes to the $\delta^{18}O_p$ depletion in eastern Brazil (SE pole) but partially contributes (44% to the total) to the $\delta^{18}O_p$ enrichment in the central-western Amazon (NW pole). Besides, local condensation changes or the local "amount effect" partially contributes (48% to the total) to the $\delta^{18}O_p$ enrichment in the central-western Amazon (NW pole) due probably to the lowering convergence height and increased rain reevaporation within a more unsaturated sub-cloud layer.

Accepted for publication in *Journal of Climate*. DOI 10.1175/JCLI-D-22-0289.1.

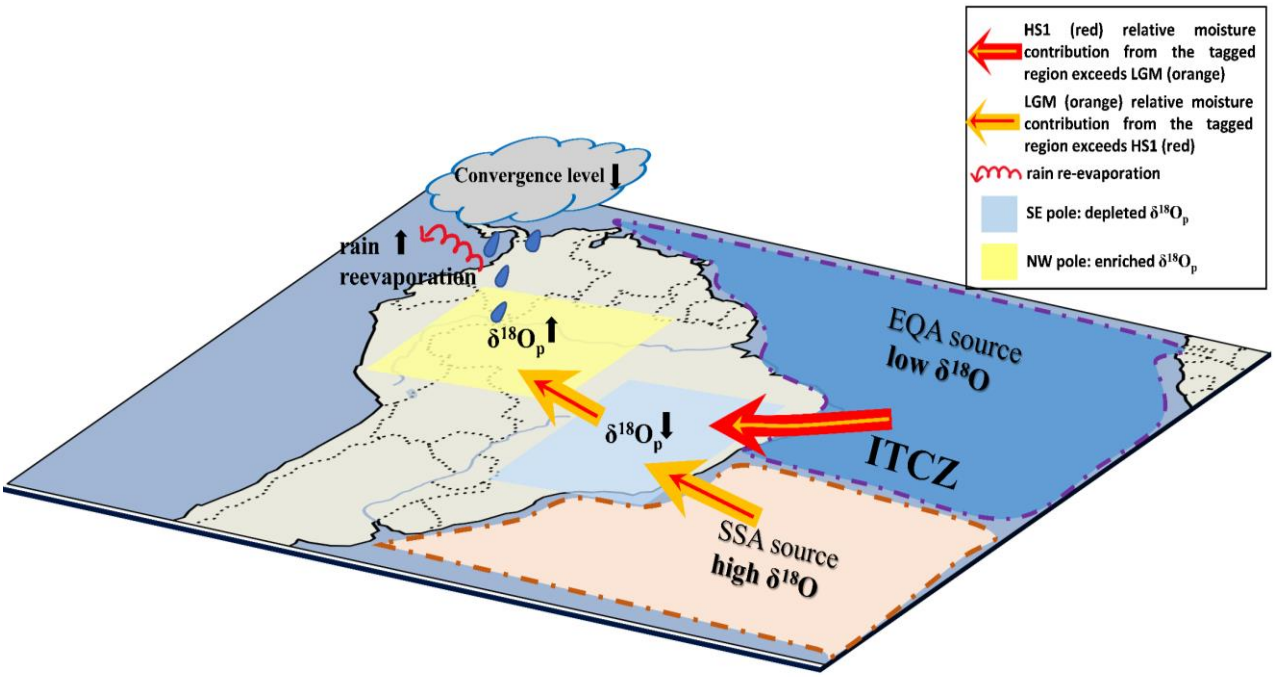

Fig. 7. Schematic figure for the mechanism of the TSA $\delta^{18}O_p$ response to increased meltwater forcing (HS1 vs. LGM). The orange (LGM) and red (HS1) arrows indicate the relative moisture contribution from each tagged region (either EQA or SSA). The width of the arrow represents the amount of contribution (the thicker the arrow, the larger the contribution). Due to increased meltwater discharge, ITCZ migrates southward, causing the switch of moisture source location from SSA to EQA, interpreting $\delta^{18}O_p$ depletion in the SE pole. In contrast, the reduced moisture contribution from the SSA and other regions partially interprets $\delta^{18}O_p$ enrichment in the NW pole. Moreover, suppressed convection lowers the local convergence height, and more unsaturated air below the sub-cloud layer increases rain reevaporation, together enriching $\delta^{18}O_p$ in the central-western Amazon.

The mechanisms below indicate that, despite a clear inverse relationship between $\delta^{18}O_p$ and rainfall amount in both dipole regions, the local "amount effect" only partially interprets the millennial $\delta^{18}O_p$ difference in the central-western Amazon (~48% to the total change), while it does not account for $\delta^{18}O_p$ change in eastern Brazil. Speleothems $\delta^{18}O$ reconstructed from eastern Brazil caves (such as Rio Grande, Paixão, and Lapa Sem Fim) are commonly thought to represent local rainfall amounts and are used to infer the past precipitation by the paleoclimate community (see Part I for detail). However, our study argues that eastern Brazil $\delta^{18}O_p$ does not document local convergence and rainfall change, but rather the isotopic composition change of water vapor ($\delta^{18}O_v$) transported into eastern Brazil due to the shifting of the moisture source location. This means that the simple negative correlation between in situ $\delta^{18}O_p$ and precipitation amount may not be adequate to indicate

Accepted for publication in *Journal of Climate*. DOI 10.1175/JCLI-D-22-0289.1.

an isotopic local amount effect, where the relationships with rainfall amount can be nonlocal and involve remote atmospheric processes that change the isotopic value of incoming water vapor. Therefore, one should be cautious in interpreting the proxy $\delta^{18}O_p$ in eastern Brazil as a signal for the past rainfall amount. More generally, we should not simply resort to the isotopic "amount effect" for past precipitation reconstruction in tropical regions without studying the associated mechanisms.

We should acknowledge that the suggested millennial dipole response of $\delta^{18}O_p$ and its associated mechanisms from our simulations may not be completely conclusive. The lack of long-term speleothem records in the Amazon region poses a challenge in directly validating the existence of the dipole or constraining its precise range on the millennial timescale across the entire TSA. Nonetheless, our conclusion finds some support from previous model simulations and other paleoclimate proxies. Specifically, millennial dipole response has been observed in snap-shot climate model simulations (Mohtadi et al., 2016, Campos et al., 2019) and in idealized meltwater forcing (or hosing) simulations (Jackson et al., 2015), in addition to our transient simulations during the last deglaciation. Other paleoclimate proxies are also consistent with our model: stabilized fluvial and eolian sediment records from the northern Amazon (Zular et al., 2019) and offshore marine sediment to the northern South America continent support a significant drying at HS1. In contrast, coastal Brazil speleothems and offshore marine sediment records (Campos et al., 2019) support a depleted $\delta^{18}O_p$ or increased precipitation at HS1. Moreover, similar dipole responses in precipitation and/or $\delta^{18}O_p$ can also be seen in interannual (Cheng et al., 2013), centennial (Orrison et al., 2022), and orbital (Cruz et al., 2009) time scales over the TSA. This suggests an inherent stability of the spatial dipole characteristics of the SASM across different timescales and external forcings, which are linked to the meridional migration of ITCZ and the South American monsoon system (see Part I for detail).

We also acknowledge that the accuracy of the water tagging technique and proposed mechanisms depends on the model's ability to reproduce the hydrological cycle. Although our model successfully reproduces the present-day seasonal cycle and $\delta^{18}O_p$ evolution during the last deglaciation over the TSA region (mostly in eastern Brazil), it underestimates the amplitude of $\delta^{18}O_p$ millennial variability compared to the speleothem proxy. (see Part I for detail). Such discrepancy between the model and proxy suggests that some dynamics or physics may not be captured by the model when focusing on specific paleoclimate events. One possible cause of model deficiency is the tropical sea surface temperature bias (not shown), which could result in the precipitation "double ITCZ" bias in the

Accepted for publication in *Journal of Climate*. DOI 10.1175/JCLI-D-22-0289.1.

tropics (Lin, 2007). Another possible origin of deficiency is the coarse model resolution, which may not be able to capture the sub-grid physics and high-frequency intense rainfall events (Goswami et al., 2017), and thus, underestimate rainfall and $\delta^{18}O_p$ magnitude in the Amazon region. Therefore, the resulting limitations of these model biases for $\delta^{18}O_p$ interpretations need to be considered and corrected in further study.

Finally, it is interesting to compare the millennial-scale hydroclimate-$\delta^{18}O_p$ variability between the SASM discussed here and the East Asian summer monsoon (EASM) (Liu et al., 2014; He et al., 2021a). In both cases, precipitation response exhibits a dipole, with an intensified monsoon wind (low-level easterly for SASM and southerly for EASM), leading to anomalous moisture convergence and, in turn, increased rainfall in the downstream pole region (i.e., western Amazon for SASM and northern China for EASM), but opposite rainfall response in the upstream pole region (i.e., eastern Brazil for SASM and southern China for EASM) (see Part I for detail). The response of $\delta^{18}O_p$ also exhibits a dipole in the tropical SASM but a monopole in EASM. The EASM exhibits coherent monopole viability in $\delta^{18}O_p$ across the entire Pan-Asian monsoon region because they are generated by the en route depletion of the single major moisture source from the Indian Ocean $\delta^{18}O_v$ (Liu et al., 2014; He et al., 2021a). In contrast, the tropical SASM region exhibits a heterogeneous $\delta^{18}O_p$ dipole variability because of the different dominant mechanisms for each pole: the change of moisture source location almost completely interprets $\delta^{18}O_p$ change in the upstream coastal region (SE pole), while moisture source location change and local condensation change, each interprets about half of the $\delta^{18}O_p$ response in the inland downstream region (NW pole).

Acknowledgments

This work is supported by U.S. NSF AGS2002506, AGS2002521. The CESM project is supported primarily by the National Science Foundation (NSF). This material is based on work supported by the National Center for Atmospheric Research, which is a major facility sponsored by the NSF under Cooperative Agreement no. 1852977. Computing and data storage resources, including the Cheyenne supercomputer (doi: 10.5065/D6RX99HX), were provided by the Computational and Information Systems Laboratory (CISL) at NCAR.

Data Availability Statement

All iTRACE simulation data can be found at:
https://www.earthsystemgrid.org/dataset/ucar.cgd.ccsm4.iTRACE.html.

References

Aggarwal, P. K., and Coauthors, 2016: Proportions of convective and stratiform precipitation revealed in water isotope ratios. *Nat. Geosci.*, **9**, 624-629, https://doi.org/10.1038/ngeo2739.

Atsawawaranunt, K., and Coauthors, 2018: The SISAL database: a global resource to document oxygen and carbon isotope records from speleothems. *Earth Syst. Sci. Data*, **11**, 1687-1713, https://doi.org/10.5194/essd-10-1687-2018.

Brady, E., and Coauthors, 2019: The connected isotopic water cycle in the Community Earth System Model version 1. *J. adv. model. earth syst.*, **11**, 2547-2566, https://doi.org/10.1029/2019MS001663.

Cruz, F. W., and Coauthors, 2005: Insolation-driven changes in atmospheric circulation over the past 116,000 years in subtropical Brazil. *Nature*, **434**, 63-66, https://doi.org/10.1038/nature03365.

Cruz, F. W., and Coauthors, 2009: Orbitally driven east–west antiphasing of South American precipitation. *Nat. Geosci.*, **2**, 210-214, https://doi.org/10.1038/ngeo444.

Cheng, H., and Coauthors, 2013: Climate change patterns in Amazonia and biodiversity. *Nat. Commun.*, **4**, 1-6, 10.1038/ncomms2415 (2013).

Campos, M. C., and Coauthors, 2019: A new mechanism for millennial scale positive precipitation anomalies over tropical South America. *Quat. Sci. Rev.*, **225**, 105990, https://doi.org/10.1016/j.quascirev.2019.105990.

Dansgaard, W., 1964: Stable isotopes in precipitation. *Tellus*, **16**, 438–468, https://doi.org/10.1111/j.2153-3490.1964.tb00181.x.

Goswami, B. B., and B. N. Goswami, 2017: A road map for improving dry-bias in simulating the South Asian monsoon precipitation by climate models. *Clim. Dyn.*, **49**, 2025-2034, https://doi.org/10.1007/s00382-016-3439-2.

Hu, J., J. Emile-Geay, C. Tabor, J. Nusbaumer, and J. Partin, 2019: Deciphering oxygen isotope records from Chinese speleothems with an isotope-enabled climate model. *Paleoceanogr. Paleoclimatol.*, **34**, 2098-2112, https://doi.org/10.1029/2019PA003741.

He, C., and Coauthors, 2021a: Hydroclimate footprint of pan-Asian monsoon water isotope during

the last deglaciation. *Sci. Adv.*, **7**, eabe2611, 10.1126/sciadv.abe2611.

He, C., Z. Liu, B. L. Otto-Bliesner, E. C. Brady, C. Zhu, R. Tomas, C. Buizert, and J. P. Severinghaus, 2021b: Abrupt Heinrich Stadial 1 cooling missing in Greenland oxygen isotopes. *Sci. Adv.*, **7**, eabh1007. 10.1126/sciadv.abh1007.

Jackson, L. C., R. Kahana, T. Graham, M. A. Ringer, T. Woollings, J. V. Mecking, and R. A. Wood, 2015: Global and European climate impacts of a slowdown of the AMOC in a high resolution GCM. *Climate Dyn*, **45**, 3299-3316, https://doi.org/10.1007/s00382-015-2540-2.

Lee, J. E., and I. Fung, 2007: "Amount effect" of water isotopes and quantitative analysis of post-condensation processes. *Hydrol. Process*, **22**, 1-8, https://doi.org/10.1002/hyp.6637.

Lee, J. E., I. Fung, D. J. DePaolo, & C. C. Henning, 2007: Analysis of the global distribution of water isotopes using the NCAR atmospheric general circulation model. *J. Geophys. Res.: Atmos.*, **112**, https://doi.org/10.1029/2006JD007657.

Lee, J. E., K. Johnson, and I. Fung, 2009: Precipitation over South America during the Last Glacial Maximum: An analysis of the "amount effect" with a water isotope- enabled general circulation model. *Geophys. Res. Lett.*, **36**, https://doi.org/10.1029/2009GL039265.

Lin, J.L., 2007: The double-ITCZ problem in IPCC AR4 coupled GCMs: Ocean–atmosphere feedback analysis. *J. Climate*, **20**, 4497-4525, https://doi.org/10.1175/JCLI4272.1.

Liu, Z., and Coauthors, 2014: Chinese cave records and East Asian Summer Monsoon. *Quat. Sci. Rev.*, **83**, 115–128, https://doi.org/10.1016/j.quascirev.2013.10.021.

Liu, X., and D. S. Battisti, 2015: The influence of orbital forcing of tropical insolation on the climate and isotopic composition of precipitation in South America. *J. Climate*, **28**, 4841-4862, https://doi.org/10.1175/JCLI-D-14-00639.1.

Mohtadi, M., M. Prange, and S. Steinke, 2016: Palaeoclimatic insights into forcing and response of monsoon rainfall. *Nature*, **533**, 191-199, https://doi.org/10.1038/nature17450.

Moore, M., Z. Kuang, and P. N. Blossey, 2014: A moisture budget perspective of the amount effect. *Geophys. Res. Lett*, **41**, 1329-1335, https://doi.org/10.1002/2013GL058302.

Neale, R. B., and Coauthors, 2010: Description of the NCAR community atmosphere model (CAM 5.0). *NCAR Tech. Note NCAR/TN-486+ STR*, **1**, 1-12.

Noone, D., 2012: Pairing measurements of the water vapor isotope ratio with humidity to deduce atmospheric moistening and dehydration in the tropical midtroposphere. *J. Climate*, **25**, 4476-4494,

https://doi.org/10.1175/JCLI-D-11-00582.1.

Nusbaumer, J., T. E. Wong, C. Bardeen, and D. Noone, 2017: Evaluating hydrological processes in the Community Atmosphere Model Version 5 (CAM5) using stable isotope ratios of water. *J. adv. model. earth syst*, **9**, 949-977, https://doi.org/10.1002/2016MS000839.

Orrison, R., and Coauthors, 2022: South American Monsoon variability over the last millennium in paleoclimate records and isotope-enabled climate models. *Clim. Past*, **18**, 2045–2062, https://doi.org/10.5194/cp-18-2045-2022, 2022.

Risi, C., S. Bony, and F. Vimeux, 2008: Influence of convective processes on the isotopic composition (δ18O and δD) of precipitation and water vapor in the tropics: 2. Physical interpretation of the amount effect. *J. Geophys. Res.: Atmos.*, **113**, https://doi.org/10.1029/2008JD009943.

Risi, C., S. Bony, F. Vimeux, C. Frankenberg, D. Noone, & J. Worden, 2010: Understanding the Sahelian water budget through the isotopic composition of water vapor and precipitation. *J. Geophys. Res.: Atmos.*, **115**, https://doi.org/10.1029/2010JD014690.

Samuels-Crow, K. E., J. Galewsky, D. R. Hardy, Z. D. Sharp, J. Worden, and C. Braun, 2014: Upwind convective influences on the isotopic composition of atmospheric water vapor over the tropical Andes. *J. Geophys. Res.: Atmos.*, **119**, 7051-7063, https://doi.org/10.1002/2014JD021487.

Tabor, C. R., and Coauthors, 2018: Interpreting precession- driven δ18O variability in the South Asian monsoon region. *J. Geophys. Res.: Atmos.*, **123**, 5927-5946, https://doi.org/10.1029/2018JD028424.

Vuille, M., R. S. Bradley, M. Werner, R. Healy, and F. Keimig, 2003: Modeling $\delta^{18}O$ in precipitation over the tropical Americas: 1. Interannual variability and climatic controls. *J. Geophys. Res.: Atmos.*, **108**, https://doi.org/10.1029/2001JD002038.

Worden, J., D. Noone, and K. Bowman, 2007: Importance of rain evaporation and continental convection in the tropical water cycle. *Nature*, **445**, 528-532, https://doi.org/10.1038/nature05508.

Wang, X., and Coauthors, 2017: Hydroclimate changes across the Amazon lowlands over the past 45,000 years. *Nature*, **541**, 204-207, https://doi.org/10.1038/nature2078.

Zular, A., and Coauthors, 2019: The role of abrupt climate change in the formation of an open vegetation enclave in northern Amazonia during the late Quaternary. *Glob. Planet. Change*, **172**, 140-149, https://doi.org/10.1016/j.gloplacha.2018.09.006.